

# The *Arabidopsis* ARCP Protein, CSI1, Which Is Required for Microtubule Stability, Is Necessary for Root and Anther Development <sup>W</sup>

Yu Mei,<sup>a,1</sup> Hong-Bo Gao,<sup>a,1</sup> Ming Yuan,<sup>b</sup> and Hong-Wei Xue<sup>a,2</sup>

<sup>a</sup>National Key Laboratory of Plant Molecular Genetics, Institute of Plant Physiology and Ecology, Shanghai Institutes for Biological Sciences, Chinese Academy of Sciences, Shanghai 200032, China

<sup>b</sup>State Key Laboratory of Plant Physiology and Biochemistry, Department of Plant Sciences, College of Biological Sciences, China Agricultural University, Beijing 100094, China

**Armadillo repeat-containing proteins (ARCPs) are conserved across eukaryotic kingdoms and function in various processes. Regulation of microtubule stability by ARCPs exists widely in mammals and algae, but little is known in plants. Here, we present the functional characterization of an *Arabidopsis thaliana* ARCP, which was previously identified as *Cellulose synthase-interactive protein1 (CSI1)*, and prove its crucial role in anther and root development. *CSI1* is highly expressed in floral tissues, and knockout mutants of *CSI1* (three allelic lines) accordingly exhibit defective anther dehiscence, which can be partially rescued by mammalian microtubule-stabilizer MAP4, suggesting that *CSI1* functions by stabilizing the microtubular cytoskeleton. *CSI1* binds microtubules in vitro, and immunofluorescence and coimmunoprecipitation studies confirmed the physical interactions between *CSI1* and microtubules in vivo. Analysis using oryzalin, a microtubule-disrupting drug, further revealed the destabilized microtubules under *CSI1* deficiency and confirmed the crucial role of *CSI1* in microtubule stability. The dynamic change of *CSI1* in response to dehydration strongly suggests the important function of *CSI1* in dehydration-induced microtubule depolymerization and reorganization, which is crucial for anther development. These results indicate the pivotal role of *CSI1* in anther development by regulating microtubule stability and hence cell morphogenesis.**

## INTRODUCTION

The Armadillo (ARM) repeat is a ~40-amino-acid-long repeated sequence motif first identified in the *Drosophila melanogaster* ARMADILLO (Riggleman et al., 1989). ARM repeat-containing proteins (ARCPs) in animal and plants function in various processes, including intracellular signaling, cytoskeletal regulation, nuclear import, transcriptional regulation, and ubiquitination (reviewed in Coates, 2003; Samuel et al., 2006). Domain prediction indicates that a superfamily of ARCPs exists in the plant kingdom. In *Arabidopsis thaliana*, there are 108 proteins containing a minimum of two ARM repeats, and these ARCPs have been divided into several subgroups based on sequence similarity and presence of other domains (Mudgil et al., 2004). In plants, some ARCPs (and their associated biological functions) have been isolated and characterized (Amador et al., 2001; Stone et al., 2003; Kim et al., 2004; Palma et al., 2005; Coates et al., 2006; Sakai et al., 2008), and most of these characterized proteins are implicated as E3 ubiquitin ligases with U-box, F-box, or Homologous to the E6-AP Carboxyl Terminus domains.

Cellulose synthase (CESA)-interactive protein1 (*CSI1*; At2g22125) (Gu et al., 2010), together with two other members, At1g44120 and At1g77460, belongs to a subfamily with an ARM-C2 domain combination specific to multicellular plants (Samuel et al., 2006). The C terminus C2 domain is believed to be involved in calcium-dependent phospholipid binding and targeting (Tanaka and Nishizuka, 1994; Duncan et al., 2000), suggesting the possible regulation of *CSI1* by other factors and the unique effect of *CSI1* in plant developmental processes.

The *Chlamydomonas* ARCP Paralyzed Flagella16 (PF16) (Smith and Lefebvre, 1996, 2000) and its mammalian homolog Sperm-associated Antigen6 (SPAG6) (Sapiro et al., 2000) were reported to be required for microtubule stability. The *Arabidopsis* ARM repeat-containing Armadillo Repeat Kinesin1 (ARK1) and ARK2, which are kinesin-related proteins, regulate root hair morphogenesis and epidermal cell expansion in a microtubule-dependent manner (Sakai et al., 2008). These findings suggest that plant ARCPs may regulate microtubules, as do their mammalian counterparts.

Microtubules are crucial for many aspects of normal plant development. The pivotal role of cortical microtubules in cell morphogenesis, especially in anisotropic cell expansion, has been well established. Mutants with abnormal cortical microtubules often show reduced anisotropic cell growth and radial cell expansion in roots and hypocotyls (Furutani et al., 2000; Whittington et al., 2001). Mutation of *Microtubule Organization1/Gemini Pollen1 (MOR1/GEM1)* resulted in disrupted anther development because of defective cytokinesis (Twell et al., 2002).

<sup>1</sup> These authors contributed equally to this article.

<sup>2</sup> Address correspondence to hwxue@sibs.ac.cn.

The author responsible for distribution of materials integral to the findings presented in this article in accordance with the policy described in the Instructions for Authors (www.plantcell.org) is: Hong-Wei Xue (hwxue@sibs.ac.cn).

<sup>W</sup>Online version contains Web-only data.

www.plantcell.org/cgi/doi/10.1105/tpc.111.095059

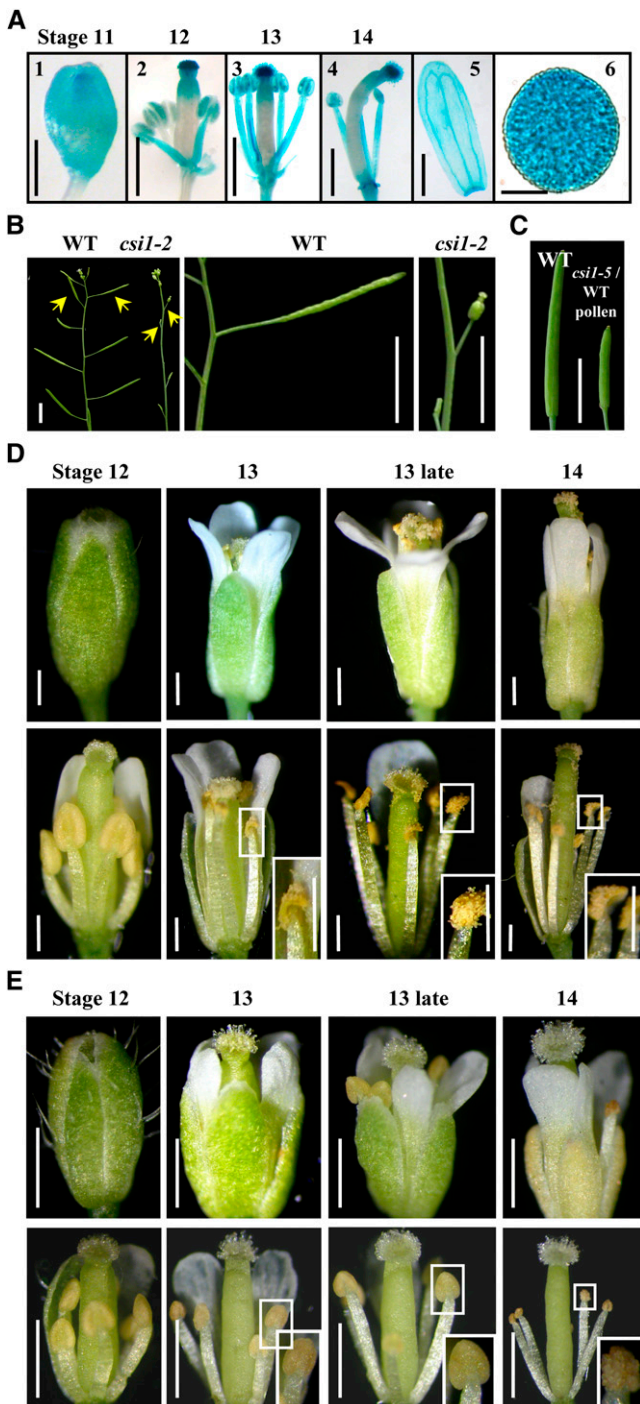


**Figure 1.** *CS1* Deficiency Results in Defective Anther Dehiscence and Complete Sterility.

**(A)** Expression of *CS1* in floral tissues at floral stages 11 to 14 (1) to (4). *CS1* is highly expressed in stigma and pollen grains (6) and modestly in sepals (5).

**(B)** Six-week-old *csil-2* plants are completely sterile. Siliques of wild-type (WT) and *csil-2* plants are indicated with arrows.

**(C)** Mature but shorter silique developed from a *csil-5* pistil manually pollinated with wild-type pollen (right) compared with a wild-type silique (left).

In higher plants, dehiscence of the anther results in the release of pollen grains, thereby ensuring pollination, subsequent fertilization, and seed setting. Anther dehiscence relies largely on the anatomy of the anther. As an important developmental process, anther dehiscence requires a series of processes, including expansion of the endothecium layer, deposition of fibrous bands in endothelial and connective cells, degradation of the tapetum and middle layers of the anther, degeneration of the septum, and the differentiation of the stomium. In addition, the epidermal cells of the anther undergo a morphological change upon maturation, and eventually all epidermal cells collapse when the anther dehisces. (Keijzer, 1987; Sanders et al., 1999; Zhao and Ma, 2000). The events leading to anther dehiscence are coordinated precisely with pollen differentiation, floral development, and flower opening for the successful pollination.

Several mutants with defects in anther dehiscence have been characterized by genetic approaches, and most of them are defective in jasmonate biosynthesis or signaling transduction (McConn and Browse, 1996; Xie et al., 1998; Sanders et al., 2000; Stintzi and Browse, 2000; Ishiguro et al., 2001; Park et al., 2002), indicating the indispensability of jasmonates in anther dehiscence. In addition, auxin perception and transport and secondary wall thickening in the endothecium are crucial for anther dehiscence (Mitsuda et al., 2005; Yang et al., 2007; Cecchetti et al., 2008). Some other mutants of transcription factors also show defects in anther dehiscence; however, the relevant mechanism is still unknown (Zhu et al., 2004; Mandaokar et al., 2006).

A recent study has identified *CS1* as a CESA-interacting protein. Mutation of *CS1* results in defective cell elongation in hypocotyls and roots, dwarf adult plants, and reduced cellulose content. The distribution and movement of CESA complexes are affected in *csil*, revealing a direct effect of *CS1* on cellulose synthesis (Gu et al., 2010). Here, through genetic and functional studies, we report the relationship between *CS1* and the microtubular cytoskeleton and confirm that *CS1* physically interacts with microtubules and plays crucial roles in root growth and anther dehiscence by regulating microtubule stability.

## RESULTS

### *CS1* Knockout Results in Complete Sterility and Defective Anther Dehiscence

Expression pattern analysis showed that *CS1* was transcribed in various tissues, including roots, stems, leaves, flowers, and seedlings, which is consistent with the recent studies by Gu et al.

**(D)** Developmental series of wild-type flowers during anther stages 12 to 14 (defined according to Sanders et al. [1999]). Intact flowers from a single inflorescence (**Top**) and the same flower with sepals and petals removed (**Bottom**) are shown. Anthers dehisced at anther stage 13 (highlighted and magnified in rectangle).

**(E)** Comparison of the *csil-2* flowers to wild-type ones at the same stages as shown in **(D)**. Anther dehiscence did not occur until anther stage 14 (highlighted and magnified in rectangle).

Bars in **(A)** (1) and (5) = 1 mm, (2) to (4) = 0.5 mm, and (6) = 5  $\mu$ m; bars in **(B)** and **(C)** = 0.5 cm; bars in **(D)** = 0.2 mm; bars in **(E)** = 0.25 mm.

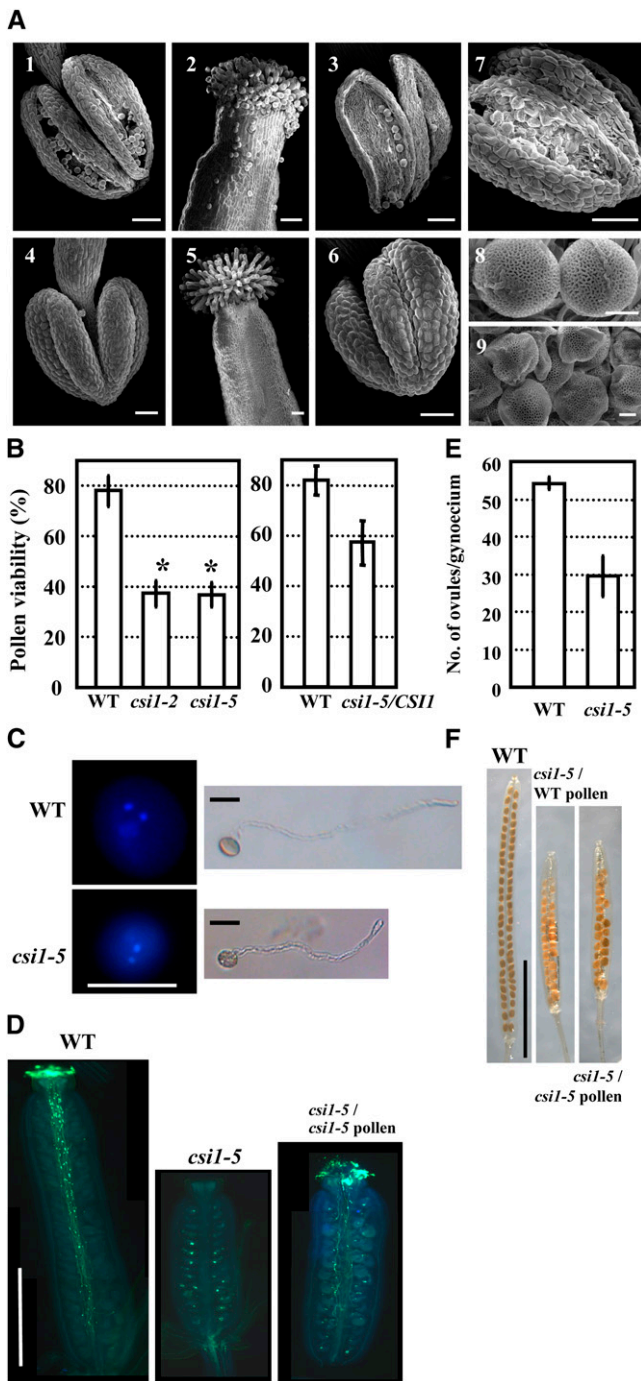


**Figure 2.** Morphological and Developmental Comparison between Wild-Type and *csi1-2* Anthers and Pollen.

**(A)** Scanning electron microscope analysis of wild-type and *csi1-2* anthers, stigmas, and pollen grains. (1), (2), (3), and (8) show wild-type floral organs. Anther at stage 13 (1); stigma (2), anther (3), and pollen grains (8) at late anther stage 13. (4) to (7) and (9) show *csi1-2* floral organs at the same stages as in the wild type.

**(B)** Pollen viability of the wild type (WT), *csi1-2*, and *csi1-5* homozygous mutant (left), and heterozygous *csi1-5/CSI1* plant (right), as determined by FDA staining. Heteroscedastic *t* tests were conducted to compare

(2010). Interestingly, a promoter-reporter gene study by fusion of the 2.0-kb promoter region of *CSI1* to the  $\beta$ -glucuronidase (GUS)-coding region revealed that *CSI1* was strongly transcribed in the stigma and pollen grains, was modestly transcribed in sepals, filaments, and anther wall, and was absent from the ovary (Figure 1A).

Furthermore, three *csi1* mutants (*csi1-2*, SALK\_122304; *csi1-4*, SALK\_047252; and *csi1-5*, SALK\_051146, equivalent to those described by Gu et al. [2010]) (see Supplemental Figure 1A online, top) were characterized and used. The T-DNA insertions result in the deficient expression of *CSI1* in homozygous mutant plants, confirmed by quantitative real-time RT-PCR analysis (see Supplemental Figure 1A online, bottom). Phenotypic observation showed that *csi1* mutant seedlings had significantly shortened primary roots (~70% reduction) and dwarf adult plants compared with the wild type (see Supplemental Figures 1B to 1D online), which is consistent with the previous study (Gu et al., 2010).

*csi1* mutant plants showed significant abnormality during reproductive growth. Observations showed that siliques of all three *csi1* alleles were small and set no seeds under normal growth conditions, indicating complete sterility under *CSI1* deficiency (Figure 1B; see Supplemental Figure 1D online). When *csi1* pistils were manually pollinated with wild-type pollen, elongated siliques could be produced with normal seeds, although the siliques were much shorter and contained fewer seeds (Figure 1C). Further detailed observations of the wild-type and *csi1-2* mutant flowers (the stages of anther development were divided according to Sanders et al. [1999]) showed that in wild-type flowers, anther dehiscence occurred at stage 13 (the time of flower opening, when the filaments had elongated to the height of the stigma to ensure successful pollination) and pollen grains were released before the full expansion of the stigmatic papilla (Figure 1D). However, buds of *csi1* were much smaller (Figure 1E, stage 12), the filaments were slightly shorter (Figure 1E, stage

pollen viability of homozygous *csi1-2*, *csi1-5*, or heterozygous *csi1-5/CSI1* with that of the wild type (\*,  $P < 0.01$ ). Error bars represent SE ( $n > 1300$ ).

**(C)** Staining of pollen grains with DAPI indicates that both wild-type and *csi1-5* pollen grains harbored one vegetative nucleus and two reproductive nuclei (left). In vitro culture of pollen grains showed that both wild-type and *csi1-5* pollen grains could germinate and elongate normally after 4 h of culture (right).

**(D)** In vivo pollen tube growth assay using aniline blue staining showed the pollen tubes in a wild-type pistil at stage 14, whereas no pollen or pollen tubes could be observed in the *csi1-5* homozygous mutant pistil. Elongated pollen tubes could be observed 6 h after manually opening the *csi1-5* anther and pollinating the pollen to the *csi1-5* pistil.

**(E)** Average number of ovules in one wild-type or homozygous *csi1-5* pistil. A heteroscedastic *t* test was conducted to compare the ovule number per pistil of *csi1* with the wild type. Error bars represent SE ( $n = 12$ ).

**(F)** Fruits developed from a *csi1-5* pistil manually pollinated with wild-type (middle) or released *csi1-5* (right) pollen compared with those developed from a wild-type pistil (left).

Bars in **(A)** (1) to (7) = 50  $\mu$ m and (8) and (9) = 5  $\mu$ m; bars in **(C)** = 10  $\mu$ m; bars in **(D)** = 0.25 cm; bars in **(F)** = 0.5 cm.

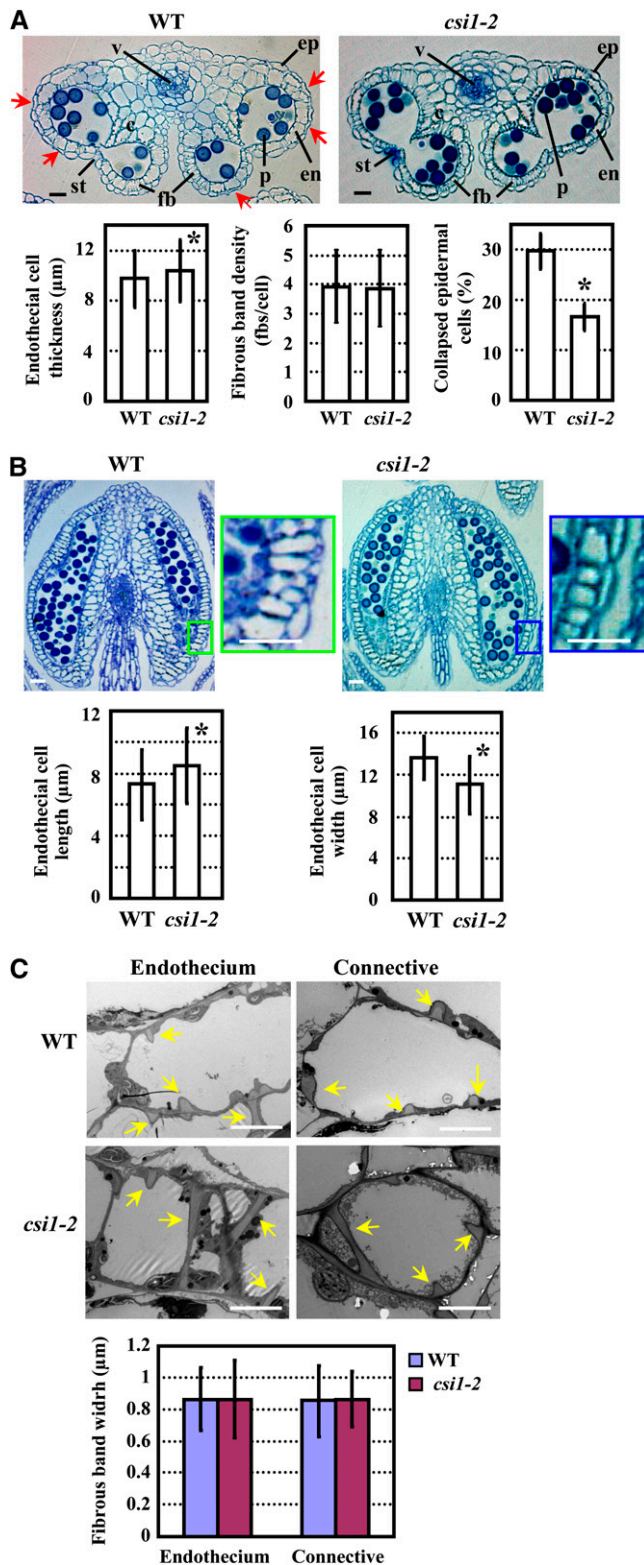


**Figure 3.** Structural Analysis of Wild-Type and *csil-2* Anthers.

**(A)** Transverse sections of wild-type (WT) and *csil-2* anthers in flower buds just before opening (**Top**) and statistical analysis of endothelial cell

thickness, fibrous band density of endothelial cells, and percentage of collapsed epidermal cells (**Bottom**). The collapsed epidermal cells in wild-type anthers are indicated with arrows. Statistical analysis was performed using a heteroscedastic *t* test (\*,  $P < 0.01$ ). Error bars represent SE ( $n > 300$ ). c, connective cells; en, endothecium; ep, epidermis; fbs, fibrous bands; p, pollen grains; st, stomium; v, vascular bundle.

**(B)** Longitudinal sections of wild-type and *csil-2* anthers in flower buds just before opening (**Top**) and statistical analysis of endothelial cell length and width (**Bottom**). Regions in the rectangles are enlarged and show endothelial cell shape. Statistical analysis was performed using a heteroscedastic *t* test (\*,  $P < 0.01$ ). Error bars represent SE ( $n > 300$ ). **(C)** Transmission electron microscope analysis of endothelial and connective cells of wild-type and *csil-2* anthers. Arrows indicate the fibrous bands deposited in the endothecium and connective cells (**Top**). Measurement of fibrous band width (**Bottom**) and statistical analysis using a heteroscedastic *t* test showed no significant difference between the wild type and *csil-2* ( $P > 0.7$ ). Error bars represent SE ( $n > 120$ ). Bars in **(A)** and **(B)** = 20  $\mu\text{m}$ ; bars in **(C)** = 5  $\mu\text{m}$ .

### **CS1 Knockouts Develop Normal Pollen Grains, and Defective Anther Dehiscence Could Not be Rescued by Exogenous Methyl Jasmonate**

In contrast with the spherical wild-type pollen grains (Figure 2A, 8), *csil-2* pollen grains were slightly smaller and stickier (hard to separate when performing manual pollination) than those of the wild type and exhibited a crumpled morphology (Figure 2A, 9). Analysis of pollen viability by fluorescein diacetate (FDA) staining showed that the pollen viability was decreased in heterozygous *csil-5* plants and was about one-half that of wild-type viability in the homozygous *csil-2* and *csil-5* plants (Figure 2B). Staining using 4',6-diamidino-2-phenylindole (DAPI) indicated the presence of one vegetative nucleus and two generative nuclei in *csil-5*

thickens, fibrous band density of endothelial cells, and percentage of collapsed epidermal cells (**Bottom**). The collapsed epidermal cells in wild-type anthers are indicated with arrows. Statistical analysis was performed using a heteroscedastic *t* test (\*,  $P < 0.01$ ). Error bars represent SE ( $n > 300$ ). c, connective cells; en, endothecium; ep, epidermis; fbs, fibrous bands; p, pollen grains; st, stomium; v, vascular bundle.

**(B)** Longitudinal sections of wild-type and *csil-2* anthers in flower buds just before opening (**Top**) and statistical analysis of endothelial cell length and width (**Bottom**). Regions in the rectangles are enlarged and show endothelial cell shape. Statistical analysis was performed using a heteroscedastic *t* test (\*,  $P < 0.01$ ). Error bars represent SE ( $n > 300$ ).

**(C)** Transmission electron microscope analysis of endothelial and connective cells of wild-type and *csil-2* anthers. Arrows indicate the fibrous bands deposited in the endothecium and connective cells (**Top**). Measurement of fibrous band width (**Bottom**) and statistical analysis using a heteroscedastic *t* test showed no significant difference between the wild type and *csil-2* ( $P > 0.7$ ). Error bars represent SE ( $n > 120$ ).

Bars in **(A)** and **(B)** = 20  $\mu\text{m}$ ; bars in **(C)** = 5  $\mu\text{m}$ .

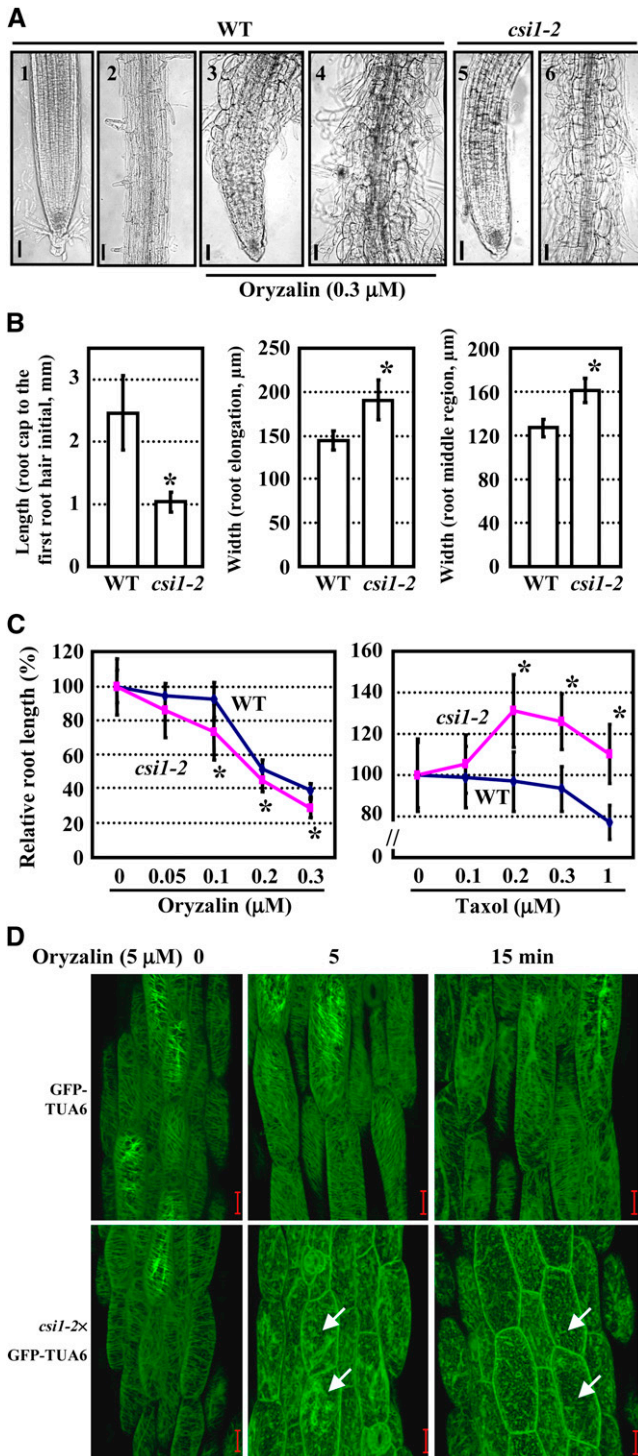


**Figure 4.** *cs1-2* Has Hypersensitive Responses to the Microtubule-Disrupting Drug Oryzalin.

**(A)** Root morphology of wild-type (WT) seedlings grown on MS medium in the presence (3) and (4) or absence (1) and (2) of 0.3  $\mu$ M oryzalin, and *cs1-2* seedlings grown on MS medium without oryzalin (5) and (6). Meristem, elongation zone (1), (3), and (5), and differentiation zone (2), (4), and (6) are shown, respectively.

pollen grains, as is the case in wild-type pollen. In addition, the viable *cs1-5* pollen germinated, and pollen tubes elongated normally in vitro (Figure 2C). Analysis by aniline blue staining of the visualized pollen tubes in vivo showed that when pollen grains of the *cs1-5* homozygous mutant were manually released from the anthers and self-pollinated to the pistil, the pollen tubes elongated normally and grew to the base of the pistil (Figure 2D, right). These results indicate that although the pollen viability was reduced, *cs1* mutant pollen developed normally to the trinucleate stage, and pollen meiosis and mitosis were not affected by *CS1* deficiency. *cs1* mutant pollen was able to fertilize the ovules, which is not a major cause of the complete sterility of *cs1* homozygous mutants.

Jasmonate and its derivatives, such as methyl jasmonate, were reported to be necessary for anther dehiscence. Application of exogenous methyl jasmonate could successfully rescue the male sterility of mutant *opr3* (Stintzi and Browse, 2000), whereas that of *cs1-2* could not be rescued (see Supplemental Figure 3 online, right). This indicates that the defective anther dehiscence and sterility were not caused by the disruption of jasmonate biosynthesis.

In addition to the altered male function, observation of *cs1-5* mutant gynoecia revealed that *cs1-5* had a decreased number of ovules per gynoecium (Figure 2E). Ovules of *cs1-5* were uniformly developed without any observed aborted ovules, and most could be fertilized by either wild-type or *cs1* pollen (Figure 2F). These results indicate that *CS1* might play a role in early gynoecial development.

#### ***CS1* Deficiency Results in Altered Anther Development**

To determine how *CS1* deficiency affects anther development, transverse and longitudinal sections of wild-type and *cs1-2* anthers were observed just before flower opening. Whereas wild-type anthers contained a substantial number of collapsed epidermal cells (resembling the shape of a concave lens with respect to the surface, whereas noncollapsed cells resemble a convex lens), only a few epidermal cells in *cs1-2* anthers displayed the same morphological change (Figure 3A). Measurements of the endothelial cell thickness (radial direction in the transverse view), which indicates the extent of expansion, length,

**(B)** Statistical analysis of the region between the proximal end of the root cap and the first root hair initial (left panel) and the width at both the elongation zone (middle panel) and middle region of the root (right panel). A heteroscedastic *t* test was performed (\*,  $P < 0.01$ ). Error bars represent SE ( $n > 40$ ).

**(C)** Statistics of the root lengths of wild-type and *cs1-2* seedlings in the presence of various concentrations of oryzalin or taxol. Primary root lengths of untreated plants were set to 100%. Heteroscedastic *t* tests were conducted to compare the different responses of *cs1-2* and wild-type seedlings to various concentrations of drugs (\*,  $P < 0.01$ ). Error bars indicate SE ( $n > 40$ ).

**(D)** Cortical microtubules of light-grown GFP-TUA6 and *cs1-2*xGFP-TUA6 hypocotyl cells after treatment with 5  $\mu$ M oryzalin for 0, 5, and 15 min, respectively. The unstable microtubules in *cs1-2* that depolymerized more rapidly are indicated with arrows.

Bars in **(A)** = 50  $\mu$ m; bars in **(D)** = 20  $\mu$ m.

and width (axial and radial direction in the longitudinal view, respectively) showed that endothelial cell length and thickness were increased and endothelial cell width was significantly reduced in *csi1-2* anthers (Figures 3A and 3B). Statistical analysis showed that fibrous band density in endothelial cells was not altered in *csi1-2* (Figure 3A). Further observation by transmission electron microscopy revealed that fibrous band widths in endothelial and connective cells were also not affected in *csi1-2* anthers (Figure 3C). These results indicate that the morphological changes in both epidermal and endothelial cells necessary for anther maturation are inhibited in *csi1-2*, which might be the cause of the defective dehiscence.

### Anisotropic Root Cell Expansion Is Inhibited in *csi1-2*

Because root growth was significantly inhibited in *csi1* seedlings, we performed a detailed analysis of *csi1-2* roots, which showed that the root morphology was distinctly abnormal, especially at the differentiation zone (Figure 4A, 1, 2, 5, 6), and root cells in *csi1-2* displayed a radially swollen morphology (Figure 4A, 6). Measurement showed that the lengths of the region between the proximal end of the root cap and the first root hair initial, an indicator of the elongation zone (Dolan et al., 1993), were shorter (Figure 4B, left panel), and the widths at both the elongation zone and middle region of the root were wider in *csi1-2* than in wild-type roots (Figure 4B, middle and right panels). These data indicate that the anisotropic expansion of root cells in *csi1-2* was inhibited.

### *csi1-2* Is Hypersensitive to the Microtubule-Disrupting Drug Oryzalin, and Microtubule-Stabilizing MAP4 Rescues the Defective Anther Dehiscence

Recent research on ARM family proteins points to a role in regulating the microtubular cytoskeleton (Smith and Lefebvre, 1996, 2000; Sapiro et al., 2000; Sakai et al., 2008). Because CSI1 was predicted to contain 16 ARM repeats, and cell swelling and growth inhibition of *csi1-2* are similar to that of wild-type seedlings treated with oryzalin (Figure 4A, 3 and 4), we explored whether the microtubular cytoskeleton was altered in *csi1-2* cells. When *csi1-2* seedlings were cultured on Murashige and Skoog (MS) medium containing oryzalin, the root growth inhibition was more pronounced than in the wild type (Figure 4C, left), whereas it was greatly suppressed by taxol treatment, a microtubule-stabilizing drug (Figure 4C, right), suggesting that CSI1, like its mammalian counterparts, could function in regulating the microtubular cytoskeleton.

To confirm the function of CSI1 in regulating the microtubular cytoskeleton, *csi1-2* was genetically crossed with an *Arabidopsis* marker line harboring CaMV35S:green fluorescent protein (GFP)-TUA6 to facilitate the observation of microtubules at the cellular level. Because GFP-TUA6 fusion proteins are not fully incorporated into cortical microtubules in root cells of *Arabidopsis* seedlings expressing GFP-TUA6 (Abe and Hashimoto, 2005), the cortical microtubules of GFP-TUA6 hypocotyl cells were observed under the absence or presence of oryzalin. As shown in Figure 4D, the organization of the cortical microtubules was not obviously different between GFP-TUA6 and *csi1-2*×GFP-TUA6

hypocotyl cells. However, when treated with 5  $\mu$ M oryzalin (for 5 min), the cortical microtubules were obviously disrupted in *csi1-2*×GFP-TUA6 seedlings, whereas microtubules in GFP-TUA6 cells seemed normal. When the treatment time was prolonged to 15 min, microtubules in the cells of *csi1-2*×GFP-TUA6 hypocotyls were significantly disrupted, whereas there was no conspicuous effect in GFP-TUA6 cells. These observations establish that sensitivity to oryzalin is increased under CSI1 deficiency, suggesting that the presence of CSI1 may be necessary for microtubule stabilization.

Furthermore, the CaMV35S:GFP-MAP4 expression cassette was transferred into *csi1-2* through genetic cross to investigate whether the defective anther dehiscence and root growth inhibition in *csi1-2* were related to microtubule instability. MAP4 is a well-characterized mammalian microtubule-associated protein and is regarded to play a role in polymerization and stability of microtubules in interphase and mitotic animal cells (Olson et al., 1995). It has been shown that expression of GFP-tagged full-length mouse MAP4 in *Arabidopsis* results in microtubule decoration in living plant cells and that the transgenic lines generating moderate-to-strong GFP fluorescence present

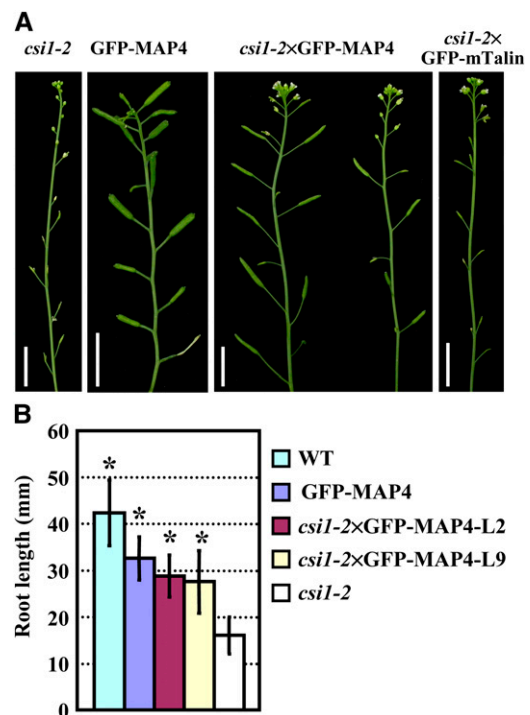


**Figure 5.** Defective Anther Dehiscence, the Sterile Phenotype, and Root Growth Inhibition Could be Rescued by Microtubule-Stabilizing MAP4.

**(A)** Inflorescence of 6-week-old *csi1-2*, GFP-MAP4, *csi1-2*×GFP-MAP4, and *csi1-2*×GFP-mTalin lines.

**(B)** Root lengths of 9-d-old wild-type (WT), GFP-MAP4, two *csi1-2*×GFP-MAP4 lines, and *csi1-2* seedlings. The statistical analysis of the wild type, GFP-MAP4, and the two *csi1-2*×GFP-MAP4 lines compared with *csi1-2* was performed using a heteroscedastic *t* tests in pairs (\*,  $P < 0.01$ ). Error bars represent SE ( $n > 40$ ).

Bars in **(A)** = 1 cm.

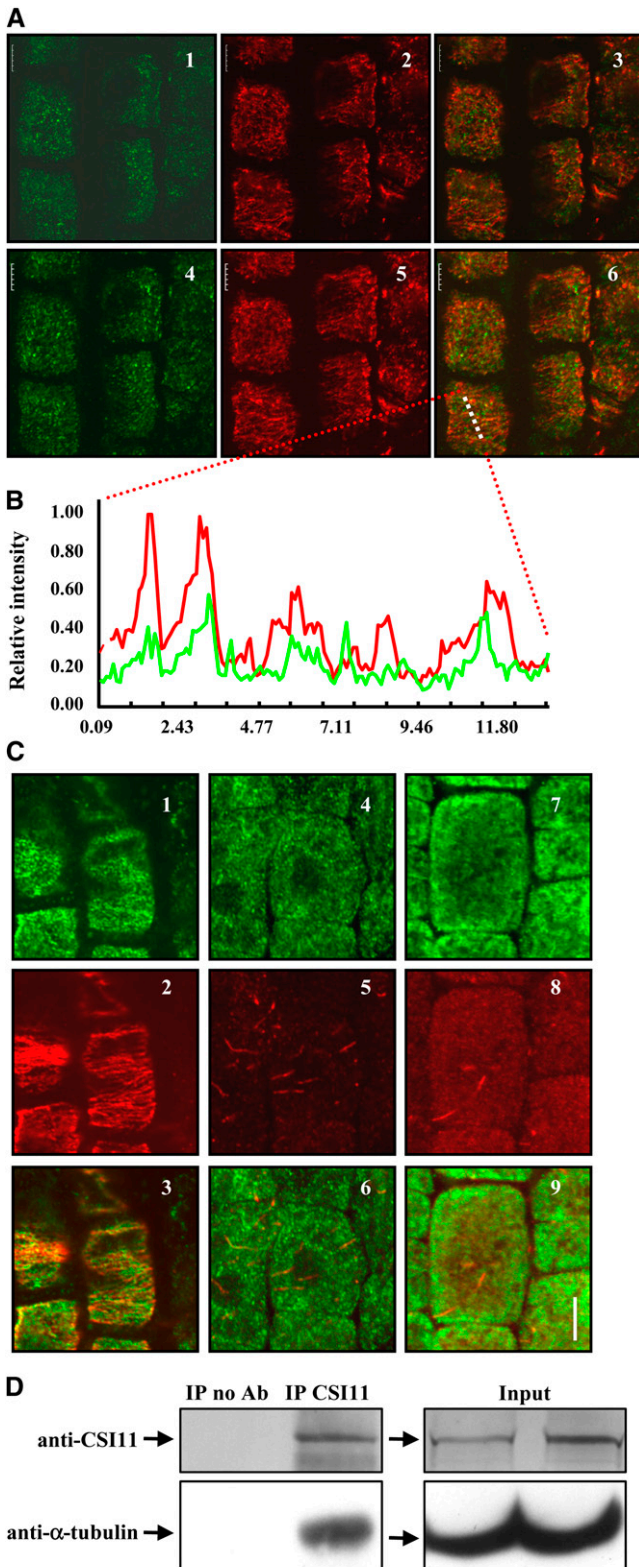


**Figure 6.** CS11 Binds to Microtubules in Vivo.

**(A)** Colocalization of CS11 and cortical microtubules in *Arabidopsis* root

several microtubule-related phenotypes, including helical and suppressed root growth, insensitivity to oryzalin, and dwarfish plants (Hashimoto, 2002) (see Supplemental Figure 4 online).

Interestingly, the *csi1-2*×GFP-MAP4 seedlings were able to set elongated siliques containing fully developed seeds, showing that defective anther dehiscence and male sterility were largely rescued (Figure 5A). The inhibition of root growth was also significantly recovered in *csi1-2*×GFP-MAP4 (Figure 5B). The recovery of male sterility and root growth inhibition by GFP-MAP4 is indeed inheritable. Overexpressing mTalin (fused to GFP), which inhibits the actin depolymerizing activity of ADF (Ketelaar et al., 2004), in *csi1-2* had no effect on the male sterile phenotype (Figure 5A). These results support the idea that defective anther dehiscence and root growth inhibition of *csi1-2* are caused by destabilization of microtubules.

### CS11 Is a Microtubule Binding Protein

The above results suggest a role for CS11 in microtubular cytoskeleton regulation. To confirm the relationship between CS11 and microtubules, we tested whether CS11 can bind to microtubules in *Arabidopsis* cells. Rabbit polyclonal antibody was raised against the N-terminal region of CS11, which recognized a band at ~220 kD in wild-type plants, the predicted molecular weight of CS11 (no such band can be detected in *csi1-2* or *csi1-5* mutants) (see Supplemental Figure 5 online). Further observation of the subcellular localization of CS11 in *Arabidopsis* root cells using immunofluorescence and two-channel confocal microscopy showed that CS11 colocalizes with microtubules and formed dot-like structures in the cortex of root epidermal cells with a broad overlap with cortical microtubules (Figure 6A). In addition, analysis of the signal intensities produced by each of the immunolabeled proteins along a randomly selected series of

cells. Immunolocalization of CS11 using anti-CS11 antibody (in green, [1] and [4]) and anti- $\alpha$ -tubulin-labeled microtubules (in red, [2] and [5]) are merged (3) and (6). Single image shot (1) to (3) and projection of 10 images at an interval of 0.2  $\mu$ m (4) to (6) are shown.

**(B)** Intensity of a plotted line by scanning through a merged region of CS11 using anti-CS11 antibody and anti- $\alpha$ -tubulin-labeled microtubules (image 6 of [A], the scanned region is highlighted by a dashed line) confirmed the correlation between CS11 and microtubules.

**(C)** Localization of CS11 after oryzalin-induced microtubule depolymerization. Immunolocalization of CS11 using anti-CS11 antibody (in green, [1], [4], and [7]) and anti- $\alpha$ -tubulin-labeled microtubules (in red, [2], [5], and [8]) are merged (3), (6), and (9). Oryzalin treatment (10  $\mu$ M) for 0 h (1) to (3), 0.5 h (4) to (6), and 4 h (7) to (9) are shown.

**(D)** Coimmunoprecipitation of CS11 and  $\alpha$ -tubulin. Four-week-old *Arabidopsis* plant extracts were immunoprecipitated with protein G conjugated beads preincubated with or without rabbit anti-CS11 antibody, followed by SDS-PAGE and immunoblot using anti-CS11 or goat anti- $\alpha$ -tubulin. Immunoprecipitation of CS11 and coimmunoprecipitation of  $\alpha$ -tubulin are shown. No cross-reactivity to eluted antibody at 25 kD or 50 kD was detected. Empty beads without antibodies were used as a negative control, and expression of CS11 and  $\alpha$  tubulin in both input extracts was examined (right panel). Ab, antibody; IP, immunoprecipitation.

Bars in **(A)** and **(B)** = 5  $\mu$ m.

pixels revealed a strong correlation between CSI1 and microtubules (Figure 6B). Further studies of the effect of microtubule depolymerization on CSI1 localization using oryzalin showed that the typical linear dots were decreased and became irregular after 30 min of oryzalin treatment (10  $\mu$ M; Figure 6C), and nearly disappeared after 4 h of treatment (some irregular, thread-like structures remained).

To further examine whether CSI1 is capable of binding to microtubules, *in vivo* coimmunoprecipitation was performed. As shown in Figure 6D, incubation of *Arabidopsis* extracts with rabbit polyclonal anti-CSI1 antibody efficiently precipitated CSI1 as detected by the same antibody. Using goat polyclonal anti- $\alpha$ -tubulin antibody, we were able to detect the coimmunoprecipitation band of  $\alpha$ -tubulin at 55 kD. No cross-activity of preadsorbed anti-goat IgG secondary antibody to eluted anti-CSI1 antibody heavy and light chains was detected. Meanwhile, incubation with empty beads as negative control did not yield the immunoprecipitation band of CSI1 and hence the coimmunoprecipitation band of  $\alpha$ -tubulin.

We further confirmed that CSI1 could directly bind to microtubules by an *in vitro* cosedimentation experiment. His-tagged full-length CSI1 was expressed in *Escherichia coli*, and purified recombinant protein was incubated with or without taxol-stabilized polymeric mammalian brain microtubules. Microtubules were pelleted, and both supernatants and pellets were analyzed by Coomassie Brilliant Blue staining. Results showed that CSI1 was significantly enriched in the pellet fraction when incubated with microtubules, whereas no CSI1 was detected in the pellet fraction when microtubules were absent, indicating that CSI1 binds directly to microtubules (Figure 7).

### Microtubules of *csi1-2* Have Altered Response to Dehydration

It has long been documented that the dehiscence program requires the dehydration of the endothecium (Keijzer, 1987; Sanders et al., 1999), and microtubules have been reported to play important roles in plant responses to dehydration (Faria et al., 2005; Lü et al., 2007). To determine whether *csi1-2* cells have an altered response of microtubules to dehydration, polyethylene glycol (PEG) 6000, which is commonly used to mimic dehydration, was used, and the microtubules in hypocotyl cells were observed under PEG6000 treatment (20%, w/v, in liquid MS media) after various time points. The results showed that the dehydration caused a depolymerization and reorganization of cortical microtubules in GFP-TUA6 hypocotyl cells (Figure 8A), which is similar to its response to cold and salt stresses (Abdrakhamanova et al., 2003; Wang et al., 2007). In GFP-TUA6 cells, the depolymerization of cortical microtubules began to become apparent at 8 h, and microtubules were mostly depolymerized at 24 h under treatment. At 36 h, the cortical microtubules seemed to be undergoing recovery, and they were fully recovered at 42 h (Figure 8A; see Supplemental Figure 6A online). By contrast, the depolymerization of cortical microtubules in the *csi1-2*×GFP-TUA6 cells, which started at 4 h and was almost complete at 8 to 12 h, was enhanced (Figure 8B; see Supplemental Figure 6B online). Similar treatment caused moderate depolymerization of cortical microtubules at 24 h and

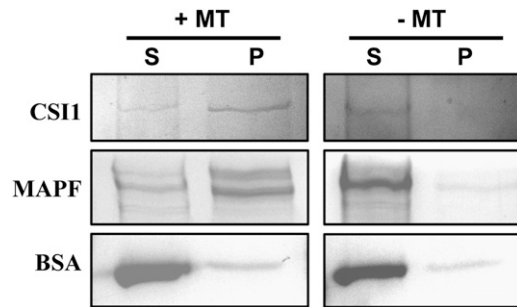


**Figure 7.** CSI1 Binds to Microtubules *In Vitro*.

Equal amounts of His-Tagged CSI1 were used in pull-down experiments in the presence (+) or absence (–) of microtubules that had been stabilized by taxol treatment. CSI1 protein was detected in the pellet [P] rather than the supernatant [S] after centrifugation. A control protein (At5g16050) showed no preferential copurification with microtubules. An isolated microtubule-associated protein fraction from bovine brain (MAPF) was used as positive control, and BSA was used as negative control. Molecular weight of bands: His-tagged CSI1, ~230 kD; MAPF (MAP1 and MAP2), ~250 kD; BSA, 68 kD.

recovery from 36 h to 42 h in GFP-MAP4 and *csi1-2*×GFP-MAP4 cells (Figure 8C, D; see Supplemental Figure 6C, D, online).

These observations support the idea that the cortical microtubules in *csi1-2* cells are unstable and that the accelerated loss of *csi1-2* cortical microtubules in the dehydration process might have an influence on the normal dehiscence program and contribute to the delay of anther dehiscence in *csi1-2*.

### Dynamics of CSI1 Localization under Dehydration

To investigate the role of CSI1 in response to dehydration and the physiological function of CSI1 and microtubule interaction, both CSI1 and microtubules were observed during PEG-induced dehydration using immunofluorescence in wild-type root cells. Compared with untreated cells, CSI1 aggregated into larger dots after 4 h of PEG treatment, and the aggregation was more significant at 8 h of treatment while the microtubule depolymerization was observed. The CSI1 particles started to disintegrate into small dots connected into lines at 12 h of treatment, and these lines were more prominent after 24 h of treatment (Figure 9). These observations indicate that the localization of CSI1 undergoes dynamic changes, as do cortical microtubules, in response to dehydration and strongly suggest a role for CSI1 in dehydration-induced microtubule depolymerization and reorganization.

### *csi1-2* Has Altered Sensitivity to Exogenous Calcium

As mentioned above, CSI1 contains a C terminus-localized C2 domain, which suggests a possible link with calcium. To confirm this, the sensitivity of *csi1-2* seedlings to exogenous calcium was tested. When wild-type seedlings were grown on MS media deficient of calcium, the primary root growth showed only ~12.5% inhibition compared with those grown on normal MS media (in which the calcium concentration is 3 mM), whereas

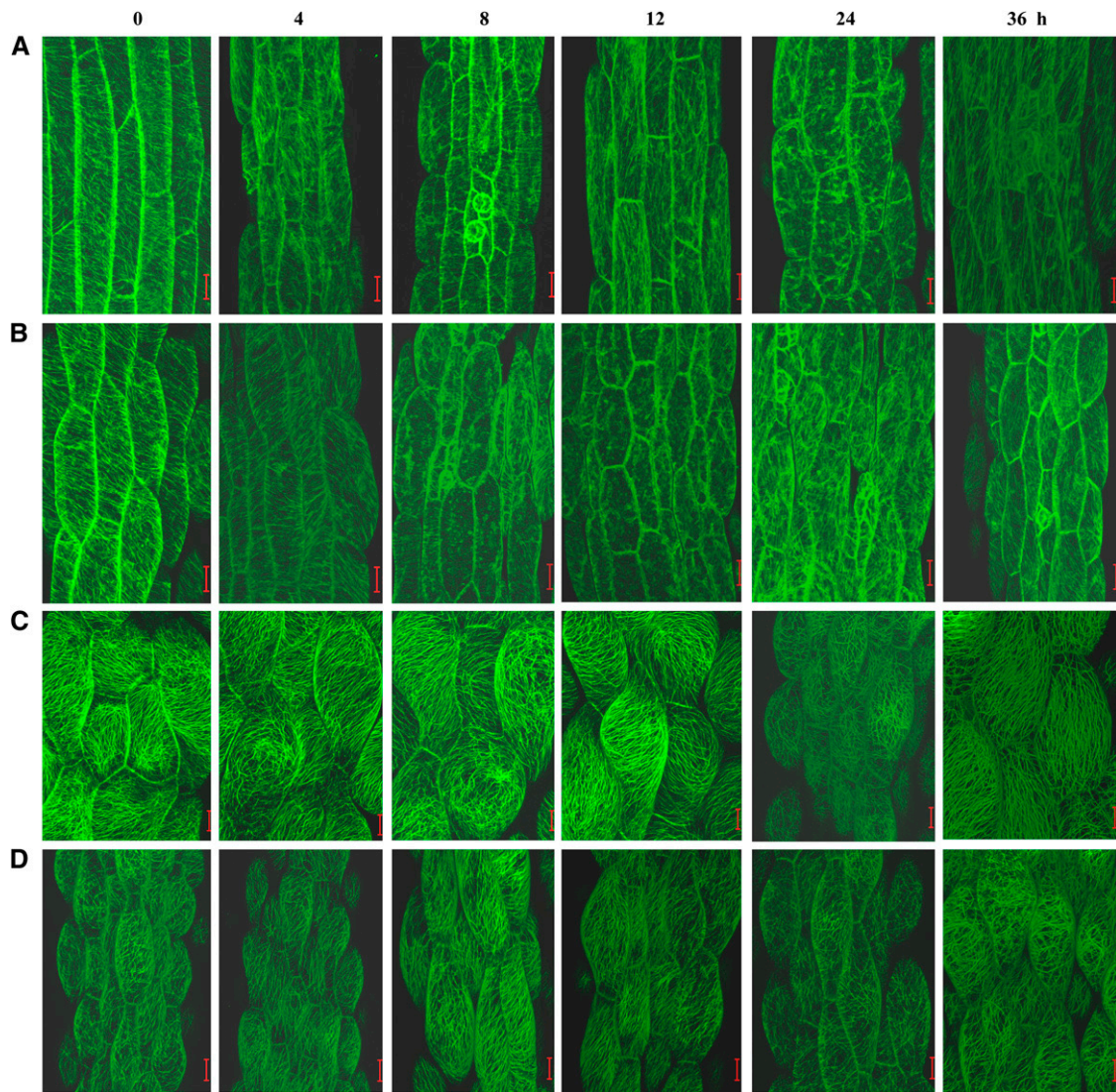


**Figure 8.** The Cortical Microtubules Depolymerized More Rapidly in *csi1-2* Cells under Dehydration Treatment.

The cortical microtubules of light-grown hypocotyl cells of 4-d-old GFP-TUA6 (A), *csi1-2*×GFP-TUA6 (B), GFP-MAP4 (C), and *csi1-2*×GFP-MAP4 (D) seedlings upon treatment with PEG6000 (20%, w/v, in liquid MS media) for 0, 4, 8, 12, 24, and 36 h, respectively. *csi1-2* showed increased depolymerization of cortical microtubules.

Bars = 20  $\mu$ m.

deprivation of calcium caused a 57.5% inhibition of *csi1-2* root growth. In addition, when grown on media supplemented with high concentrations of calcium, the inhibitory effect on root growth was more severe in *csi1-2* seedlings than wild-type ones (Figure 10). These results show that primary root growth of *csi1-2* was more sensitive to exogenous calcium at both stimulatory and inhibitory concentrations.

## DISCUSSION

Proteins containing ARM repeats exist widely among unicellular eukaryotes, animals, and plants. The function and mechanism of several animal ARCPs have been relatively well characterized.

However, their functions are largely unknown in higher plants, except for a few members (reviewed in Coates, 2003; Samuel et al., 2006). Structural analysis indicates the presence of an ARM-C2 domain combination of CSI1, which is unique to multicellular plants. This unique domain organization suggests that CSI1 might be important for a plant-specific process.

*CSI1* is widely expressed in male and female floral organs, suggesting the important role of CSI1 during reproductive development. Indeed, homozygous *csi1* mutants are completely sterile, and the *csi1* mutation was found to result in three major defects, including decreased pollen viability and ovule numbers per gynoecium and defective anther dehiscence, which results in complete sterility of the homozygous mutant. When *csi1* mutant

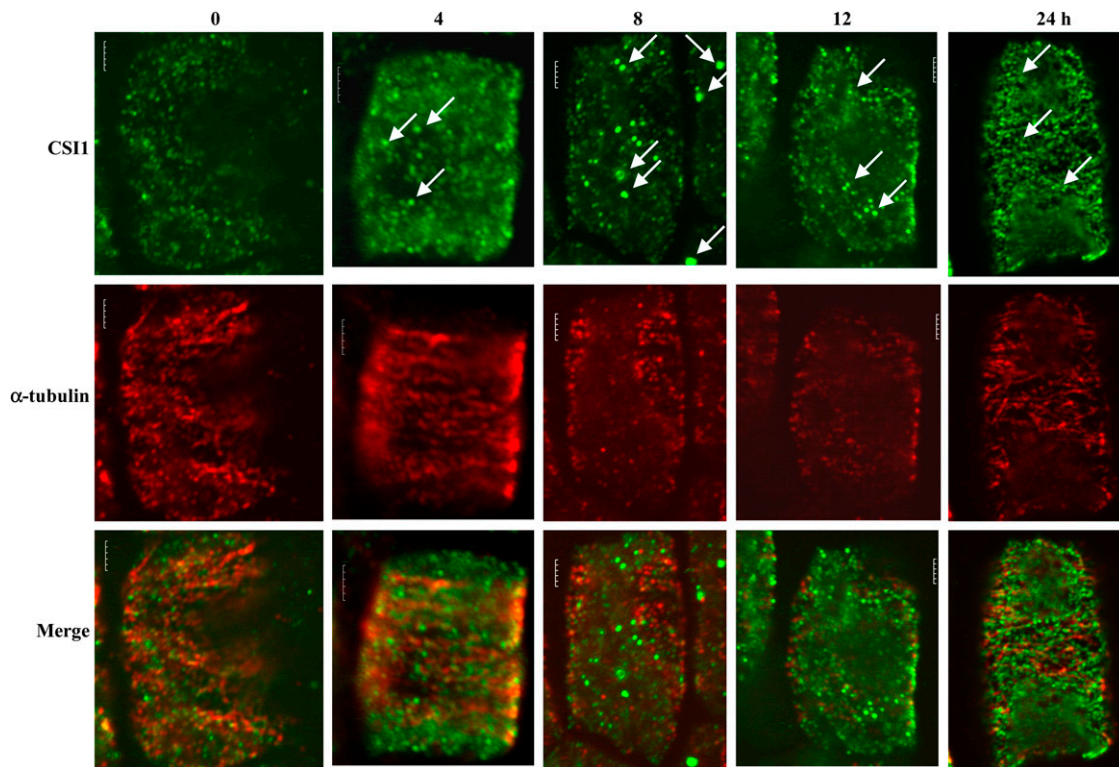


**Figure 9.** Dynamic Change of CSI1 and Microtubules under Dehydration Treatment.

Immunolocalization of CSI1 using anti-CSI1 antibody (green) and anti- $\alpha$ -tubulin-labeled microtubules (red) of wild-type root cells exposed to treatment with PEG6000 (20%, w/v, in liquid MS media) for 0, 4, 8, 12, and 24 h, respectively. Arrows indicate the induced aggregation of CSI1 after dehydration treatment.

Bars = 5  $\mu$ m.

anthers were opened mechanically and the released pollen grains were used for self-pollination, pollen tubes grew normally, and elongated siliques with fully developed seeds formed. It is thus supposed that the sterility is caused by the defective anther dehiscence. Both epidermal and endothelial cells undergo morphological changes during anther maturation (Evans and Brown, 1989; Sanders et al., 1999). The reduced and collapsed epidermal cells and the different extent of endothecium expansion in *csi1* indicate a delay in anther maturation in *csi1* (perhaps caused by a delay in differentiation), which might account for the defective anther dehiscence. In addition, root growth is significantly inhibited in *csi1* because of isotropic cell expansion, resulting in a shorter elongation zone, radially swollen cells, and wider roots. These results indicate that the *csi1* phenotype is probably caused by a defect in cell morphogenesis, and it is thus concluded that CSI1 is indispensable for anther development, especially for anther dehiscence and anisotropic root cell expansion. Because cortical microtubules play a pivotal role in cell morphogenesis (Furutani et al., 2000; Whittington et al., 2001), the fact that microtubules are unstable in *csi1* further supports the conclusion.

Pharmacological experiments revealed the reduced stability of microtubules in *csi1* seedlings and suggested a link to the root phenotype. Expression of microtubule-stabilizing MAP4 in *csi1*

partially rescued the defective anther dehiscence and root growth. In addition, taxol could also partially rescue the root growth inhibition in *csi1*, presumably by stabilizing microtubules. These results support the hypothesis that microtubules are less stable in *csi1* and that CSI1 is necessary for microtubule stabilization. Studies in alga and mammalian ARCPs show that the ARM repeats can bind and stabilize microtubules (Smith and Lefebvre, 1996, 2000; Sapiro et al., 2000). We also note that the ARM repeat is closely related to the HEAT repeat, which is found in the MAPs, SPR2 (Buschmann et al., 2004; Shoji et al., 2004), and MAP215 family proteins (Whittington et al., 2001; Konishi and Sugiyama, 2003; Hamada et al., 2004) that can bind and stabilize microtubules in plants. CSI1 directly binds to microtubules in vitro, and subcellular localization studies by immunofluorescence observation and coimmunoprecipitation analysis confirmed the microtubule localization and binding of CSI1, providing direct evidence of the association of CSI1 with microtubules and thereby demonstrating that a plant ARCP functions as a microtubule binding protein that stabilizes the microtubule cytoskeleton, similar to mammalian ARCPs.

In addition, it has been reported that changes in microtubule and secondary cell wall organization induced by glyphosate in endothelial cells inhibit the anther dehiscence in cotton, which highlights the importance of microtubular function in the

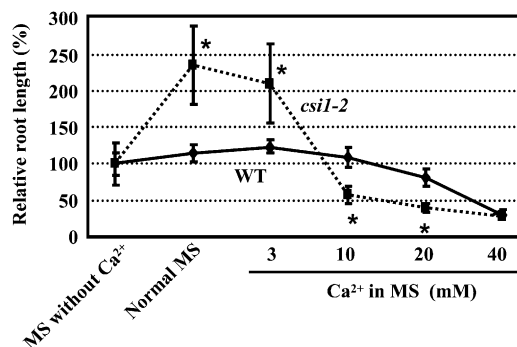


**Figure 10.** *cs1-2* Is Hypersensitive to Exogenous Calcium.

Seeds of wild-type (WT) and heterozygous mutant (*cs1-2/CSI1*) plants were germinated and grown vertically on MS medium without calcium for 4 d, and then wild-type and selected homozygous *cs1-2* seedlings were transferred to medium supplemented with different concentrations of calcium for another 8 d. Primary root lengths of plants grown on MS medium without calcium were set to 100%. Heteroscedastic *t* tests were conducted to compare the different response of *cs1-2/CSI1* and the wild type at various concentrations of treatments (\*,  $P < 0.01$ ). Error bars indicate SE ( $n > 40$ ).

dehiscence program (Yasuor et al., 2006). Our observation reveals that microtubules in *cs1* cells are depolymerized more rapidly under dehydration for 4 to 12 h (this time period is sufficient for anther dehydration, bud opening, and anthesis in wild-type anthers) (Smyth et al., 1990). Because dehydration is indispensable for anther dehiscence (Keijzer, 1987; Sanders et al., 1999) and microtubules are involved in the plant's response to dehydration (Faria et al., 2005; Lü et al., 2007), this defect might reflect a possible disruption in anther dehydration or plant drought resistance of *cs1*. CSI1 exhibits interesting dynamics under dehydration treatment; it initially forms large particles but resumes cortical microtubule colocalization and organization into lines when treatment time is prolonged. Considering the dynamic reorganization of the cortical microtubule itself, this strongly suggests a connection between CSI1 and microtubule behavior under dehydration and strongly supports the hypothesis that CSI1 has a function in regulating microtubule stability.

A recent study demonstrated that CSI1 is required for cell elongation by interacting with the CESA complex and regulating cellulose biosynthesis (Gu et al., 2010). As early as the 1970s, it was suggested that mobile cellulose-synthesizing complexes somehow traveled along or between the underlying microtubules as guide rails (reviewed in Heath and Seagull, 1982). Since then, many studies with both drugs and mutants have supported the microfibril guidance hypothesis with observations of parallelism between microtubules and cellulose (reviewed in Baskin, 2001). Although exceptions exist, it is widely accepted that cortical microtubules are closely related to the cell wall biosynthesis machinery, and the visualization of dynamic CESA6 complexes provide strong supporting evidence for this (Paredes et al., 2006). However, how cortical microtubules and the cell wall biosynthesis machinery are connected remains to be determined. The ability of CSI1 to bind both CESA and microtubules suggests that

CSI1 could be this important missing component. Further studies are needed to elucidate the role of CSI1 in microtubule–CESA interactions, especially in the guidance of CESA by microtubules.

Furthermore, *cs1* showed altered sensitivity to both low and high concentrations of exogenous calcium in primary root growth compared with wild-type seedlings, suggesting possible roles for the C2 domain in calcium signaling and indicating that calcium may be involved in the CSI1-mediated regulation of microtubule stability and anther dehiscence.

In conclusion, we have demonstrated that CSI1 is necessary for root growth and anther dehiscence by regulating microtubule stability and hence cell morphogenesis.

## METHODS

### Plant Materials, Growth Conditions, and Measurement of Root Length

*Arabidopsis thaliana* ecotype Columbia was used in the study. An *Arabidopsis* GFP-TUA6 line expressing GFP-tagged TUA6 (At4g14960; Ueda et al., 1999) and GFP-MAP4 line expressing GFP-tagged full-length mouse MAP4 were used for microtubule observation. The *opr3* mutant was used to test the function of methyl jasmonate. Plant transformation was performed using the floral dip method (Clough and Bent, 1998). Seeds were surface-sterilized with 20% (v/v) bleach and sown on plates containing MS salts. One-week-old seedlings were transferred to soil and grown at 22°C under a 16-h light/8-h dark photoperiod. For root length measurement, plates were placed vertically, and root lengths were measured 9 d after germination. All measurements were performed using triplicate biological samples, and results are presented as averages of at least 30 seedlings.

### Quantitative Real-Time RT-PCR Analysis

Ten-d-old homozygous seedlings were harvested for RNA extraction. PCR amplification was executed with the RotorGene 3000 system (Corbett Research) using the SYBR green detection protocol (Toyobo). *ACTIN7* was used as an internal control. Primers used were as follows: *CSI1* (5'-GTAACAACATGAAGCAATCCGTTG-3' and 5'-TTGTTCTTGCATGAAATGTGGAG-3', nucleotide position 6116 to 6139 or 6277 to 6299 of the *CSI1* coding sequence, respectively), and *ACTIN7* (5'-TTCCGTTCTGCGGTAGTGG-3' and 5'-CCGGTATTGTGCTCGATCTG-3').

### Promoter-GUS Fusion Studies

The ~2.0-kb *CSI1* promoter region was amplified by PCR using primers CSI1p-1 (5'-CCCAAGCTTCCAAATCGGAACATAATAGAAAC-3', *Hind*III site underlined) and CSI1p-2 (5'-CGGGATCCCTCAAATCAAAGTAGACCCAG-3', *Bam*HI site underlined) with *Arabidopsis* genomic DNA as template. The resulting DNA fragment was subcloned into pCAM-BIA1300+pBI101.1 (Liu et al., 2003), and the resultant construct was transformed into *Arabidopsis*. Positive transgenic plants were selected through hygromycin resistance screening (30 μg/mL) and independent lines of T2 and T3 homozygous progenies were used for detecting GUS activities (Jefferson et al., 1987). Photography was performed using a Nikon microscope (SMZ800) with a digital camera (Nikon Coolpix 4500).

### Identification of *CSI1* Knockout Mutants

Three putative knockout mutants of *CSI1*, SALK\_122304, SALK\_047252, and SALK\_051146, were identified in the Salk Institute T-DNA insertion

library database (<http://signal.salk.edu/cgi-bin/tdnaexpress>; Alonso et al., 2003) by searching with locus At2g22125. For each mutant, two pairs of primers were used in PCR amplification to confirm the presence of T-DNA and to identify the homozygous mutant lines. CSI1-1 (5'-ATCAGGTCCACCACGGTTCCA-3', nucleotide position 6033 to 6053 of the *CSI1* coding sequence) together with CSI1-2 (5'-TCCCAGCATCAC-CACCCTATC-3', nucleotide position 6346 to 6366 of the *CSI1* coding sequence), and CSI1-1 with LBa1 (5'-TGGTTCACGTAGTGGGCCATCG-3', according to Salk Institute protocol) were used for line SALK\_122304. CSI1-3 (5'-AATGTCCTGAAGAACAACCCAC-3', nucleotide position 5494 to 5516 of the *CSI1* coding sequence) with CSI1-4 (5'-GACTA-CCAGAGTACCTGGCAAAC-3', nucleotide position 6079 to 6102 of the *CSI1* coding sequence), and CSI1-4 with LBa1 were used for line SALK\_047252. CSI1-5 (5'-TGTGCCAAATTCGTTCAAGC-3', nucleotide position 2902 to 2017 of the *CSI1* coding sequence) with CSI1-6 (5'-TCGCCTTTCGAGAAAGTAGCC-3', nucleotide position 3573 to 3592 of the *CSI1* coding sequence), and CSI1-6 with LBa1 were used for line SALK\_051146. Because the homozygous mutants were male sterile, seeds of heterozygous lines were used for homozygote screening in further studies.

### Microscopic Observation

Bright-field micrographs of individual flowers and siliques (cleared by H<sub>2</sub>O: arabic gum:glycerol:chloralhydrate = 6:1.5:1:20 for 15 min) were taken using a Nikon dissecting microscope (SMZ800) with a digital camera (Nikon Coolpix 4500). For observation of transverse and longitudinal sections of anthers, samples were fixed in formalin, acetic acid, and ethanol solution (50% ethanol:glacial acetic acid:formaldehyde = 90:5:5, v/v/v), dehydrated with a graded ethanol series, and then embedded into Epon812-resin. After polymerization at 60°C, 3- $\mu$ m-thick sections were prepared and stained with toluidine blue. The fibrous bands per endothelial cell and the number of collapsed epidermal cells were counted, and the endothelial cell length, width, and thickness were measured with the aid of the program ImageJ (version 1.34 for Windows; <http://rsb.info.nih.gov/ij/>). At least 300 cells from five different anthers were used for each measurement.

Transmission electron microscopy analysis was performed to observe the fibrous band width of endothelial and connective cells. Samples were fixed, processed, and embedded in Epon812-resin. Sections (60-nm) were cut in series with an ultramicrotome (Leica EM UC6) and stained with uranyl acetate and lead citrate. The sections were examined with a Hitachi H7650 electron microscope at 80 kV.

To determine the pollen viability, pollen grains were treated with 100  $\mu$ g/mL FDA (Sigma-Aldrich) for 10 min and observed by fluorescence microscopy. Pollen grains with strong fluorescence (excitation wavelength, 488 nm) were scored as viable. To monitor pollen development, pollen grains were treated with DAPI (Sigma-Aldrich) solution (with a final concentration of 2  $\mu$ g/mL dissolved in 7% Suc, w/v) for 5 min and viewed by fluorescence microscopy under UV light excitation.

An in vitro pollen tube growth assay was performed by culturing the pollen grains on medium [18% Suc, 0.01% boric acid, 1 mM CaCl<sub>2</sub>, 1 mM Ca(NO<sub>3</sub>)<sub>2</sub>, 1 mM MgSO<sub>4</sub>, and 0.5% agar] (Lalanne et al., 2004). Plates were incubated for 4 h at 22°C under continuous light, and pollen tubes were photographed. For in vivo pollen tube growth observation, pistils were fixed in acetic acid/ethanol (1:3) solution followed by softening in 8 M NaOH and stained with aniline blue.

For scanning electron microscopy analysis, samples of wild-type and *csi1* flower bud clusters were fixed in formalin, acetic acid, and ethanol solution for 24 h, dehydrated with a graded ethanol series, and dried at critical point in liquid CO<sub>2</sub>. Samples were coated with gold and then examined in an S-4160 Field Emission Scanning Electron Microscope (Hitachi) at an accelerating voltage of 10 kV.

Confocal microscopy observations and image acquisition were performed using a Zeiss LSM 510 META. Hypocotyl epidermal cells of 4-d-old light-grown *Arabidopsis* seedlings containing GFP-TUA6 fusion proteins or *csi1-2*×GFP-TUA6 seedlings generated by genetic cross were used to observe microtubules.

### Methyl Jasmonate Treatment

Flowering inflorescences of 6-week-old *csi1-2*, *opr3*, and wild-type plants were tagged, and all opened flowers were removed. The remaining flower bud clusters were dipped into an aqueous solution of 500  $\mu$ M methyl jasmonate (Sigma-Aldrich) or water (both containing 0.1% Tween-20) twice a day (morning and night) for 3 d. Photographs were taken 1 week after treatment.

### Treatment with Microtubule-Disrupting or -Stabilizing Drugs or PEG6000

Four-d-old seedlings grown on vertical plates containing standard MS medium were transferred to plates containing MS medium with various concentrations (0, 0.05, 0.1, 0.2, or 0.3  $\mu$ M) of the microtubule-disrupting drug oryzalin (3,5-dinitro-N<sub>4</sub>,N<sub>4</sub>-dipropylsulfanilamide; Sigma-Aldrich) or microtubule-stabilizing drug taxol (Paclitaxel; Invitrogen). After another 5 d, root lengths and widths were measured with the aid of the program ImageJ. At least 40 roots grown on each plate were measured to calculate mean lengths with SE.

Upper hypocotyls of 4-d-old light-grown seedlings of transgenic *Arabidopsis*-expressing GFP-tagged TUA6 in both the wild type and *csi1-2* with GFP-TUA6 background were used for cortical microtubule observation. Oryzalin (5  $\mu$ M) was applied to the whole plant for 5 or 15 min. For dehydration treatment, seedlings were treated with PEG6000 (20%, w/v, in liquid MS media) for 0, 4, 8, 12, 24, 36, or 42 h. The hypocotyls were cut off immediately before the observation.

### Expression of the His-CSI1 Fusion Protein and in Vitro Microtubule Binding Assay

Two overlapping fragments of *CSI1* coding sequence (1 to 3600 and 3491 to 6450 from ATG) were amplified from ecotype Columbia cDNA using primers CSI1-q-s (5'-ATGACAAGTGCTCTTGGATGGAGAT-3'), CSI1-q-a (5'-TAAGGGAATCGCCTTTTCGAGAAGTA-3'), and CSI1-h-s: (5'-GTC-GCAGGAGTTTACTTTAGTGC-3'), CSI1-h-a (5'-CTTGTAGACCCTG-GAATTCTATCTC-3'), respectively. The amplified fragments were sequenced to verify the accuracy and were combined to the whole *CSI1* cDNA by the endogenous *SexAI* (*Csil*) restriction site (3523 nucleotides from ATG). The obtained whole *CSI1* coding region was then cloned into the pET32a vector, and expression and purification of *CSI1* in *Escherichia coli* was performed as previously described (Liu et al., 2003).

An in vitro microtubule-binding assay was performed according to the previous description (Pignocchi et al., 2009). Briefly, 5  $\mu$ g purified His-*CSI1* protein was incubated with 10  $\mu$ g prepolymerized bovine brain tubulin in general tubulin buffer (80 mM PIPES, pH 7.0, 2 mM MgCl<sub>2</sub>, and 0.5 mM EGTA) containing 20  $\mu$ M taxol followed by centrifugation at 100,000g, and both soluble and pellet fractions were analyzed by SDS-PAGE and Coomassie Brilliant Blue staining. Tubulin protein, control proteins, and chemical reagents were obtained from Cytoskeleton.

### Immunofluorescence and Coimmunoprecipitation

Rabbit polyclonal antibody was produced by IMMUNOGEN BIOLOGICAL TECHNOLOGY. The N terminus region (1 to 333 amino acids) of *CSI1* was expressed, purified, and used as immunogen. Antibody product was affinity-purified by antigen and confirmed to recognize 10 pg antigen in immunoblot analysis.

Untreated or PEG-treated seedlings were immunostained as described previously (Robert et al., 2005). Briefly, 4- to 7-d-old wild-type seedlings were fixed and penetrated followed by incubation of primary antibodies (anti-CSI1 diluted 1:100, anti- $\alpha$ -tubulin [Abcam] diluted 1:500) overnight. After washing, Alexa 488 (Invitrogen) and CY3 (Abcam) conjugated secondary antibodies (diluted 1:200) were applied, incubated, and washed. The final mounted slides were observed using Fluoview FV10i (Olympus) confocal microscope.

Coimmunoprecipitation using rabbit polyclonal anti-CSI1 antibody was performed as described (Drykova et al., 2003). Briefly, anti-CSI1 antibody was incubated with Protein G conjugated beads (Invitrogen) followed by incubation of wild-type cell extracts at room temperature for 1 h. After washing and elution, the precipitated proteins were separated by SDS-PAGE and detected by immunoblot using anti- $\alpha$ -tubulin antibody (Santa Cruz).

#### Accession Numbers

Sequence data generated or used in this study can be found in the EMBL/GenBank database under the following accession numbers: *CSI1* (At2g22125, NM\_127781) and *ACTIN7* (At5g09810, NM\_121018).

#### Supplemental Data

The following materials are available in the online version of this article.

**Supplemental Figure 1.** Identification and Phenotypic Analysis of *CSI1* Knockout Mutants.

**Supplemental Figure 2.** Scanning Electron Microscope Analysis of Anthers and Pollen Grains of Wild-Type and *csi1-5* Plants.

**Supplemental Figure 3.** Exogenous Methyl Jasmonate (MeJA) Could Not Rescue the Sterile Phenotype of *csi1-2* (Right Panel), whereas *opr3* Regained Fertility upon Treatment with MeJA (Left Panel).

**Supplemental Figure 4.** Growth of MAP4 Seedlings.

**Supplemental Figure 5.** Validation of anti-CSI1 Antibody.

**Supplemental Figure 6.** Cortical Microtubules in Hypocotyl Cells of 4-d-old GFP-TUA6 (A), *csi1-2*×GFP-TUA6 (B), MAP4 (C), and *csi1-2*×MAP4 (D) Seedlings under PEG6000 (20%, w/v) Treatment for 42 h.

#### ACKNOWLEDGMENTS

We thank Professor Clive Lloyd at the John Innes Centre for critical reading, editing, and comments on the article. We thank Zhenbiao Yang and Bo Liu for providing the *Arabidopsis* GFP-TUA6 seeds, Chuan-You Li for providing the seeds of *opr3*, Jian Xu for providing the *Arabidopsis* GFP-MAP4 seeds, and the Salk Institute Genomic Analysis Laboratory for providing T-DNA insertion mutant lines. We also thank Xiao-Yan Gao for help on scanning electron microscope observation and section analysis. This article was supported by State Key Project of Basic Research (2012CB944804).

#### AUTHOR CONTRIBUTIONS

Y.M. identified the *csi1* mutants and analyzed the phenotype. H.-B.G. demonstrated the interaction between CSI1 and microtubules and helped analyze the phenotype of mutants. M.Y. helped study the interaction between CSI1 and microtubules. H.-W.X. designed the experiments and wrote the article.

Received December 19, 2011; revised January 21, 2012; accepted March 1, 2012; published March 16, 2012.

#### REFERENCES

- Abdrakhamanova, A., Wang, Q.Y., Khokhlova, L., and Nick, P. (2003). Is microtubule disassembly a trigger for cold acclimation? *Plant Cell Physiol.* **44**: 676–686.
- Abe, T., and Hashimoto, T. (2005). Altered microtubule dynamics by expression of modified alpha-tubulin protein causes right-handed helical growth in transgenic *Arabidopsis* plants. *Plant J.* **43**: 191–204.
- Alonso, J.M., et al. (2003). Genome-wide insertional mutagenesis of *Arabidopsis thaliana*. *Science* **301**: 653–657.
- Amador, V., Monte, E., García-Martínez, J.L., and Prat, S. (2001). Gibberellins signal nuclear import of PHOR1, a photoperiod-responsive protein with homology to *Drosophila* armadillo. *Cell* **106**: 343–354.
- Baskin, T.I. (2001). On the alignment of cellulose microfibrils by cortical microtubules: A review and a model. *Protoplasma* **215**: 150–171.
- Buschmann, H., Fabri, C.O., Hauptmann, M., Hutzler, P., Laux, T., Lloyd, C.W., and Schäffner, A.R. (2004). Helical growth of the *Arabidopsis* mutant *tortifolia1* reveals a plant-specific microtubule-associated protein. *Curr. Biol.* **14**: 1515–1521.
- Cecchetti, V., Altamura, M.M., Falasca, G., Costantino, P., and Cardarelli, M. (2008). Auxin regulates *Arabidopsis* anther dehiscence, pollen maturation, and filament elongation. *Plant Cell* **20**: 1760–1774.
- Clough, S.J., and Bent, A.F. (1998). Floral dip: A simplified method for *Agrobacterium*-mediated transformation of *Arabidopsis thaliana*. *Plant J.* **16**: 735–743.
- Coates, J.C. (2003). Armadillo repeat proteins: Beyond the animal kingdom. *Trends Cell Biol.* **13**: 463–471.
- Coates, J.C., Laplaze, L., and Haseloff, J. (2006). Armadillo-related proteins promote lateral root development in *Arabidopsis*. *Proc. Natl. Acad. Sci. USA* **103**: 1621–1626.
- Dolan, L., Janmaat, K., Willemsen, V., Linstead, P., Poethig, S., Roberts, K., and Scheres, B. (1993). Cellular organization of the *Arabidopsis thaliana* root. *Development* **119**: 71–84.
- Drykova, D., Cenklová, V., Sulimenko, V., Volc, J., Dráber, P., and Binarová, P. (2003). Plant gamma-tubulin interacts with alphabeta-tubulin dimers and forms membrane-associated complexes. *Plant Cell* **15**: 465–480.
- Duncan, R.R., Shipston, M.J., and Chow, R.H. (2000). Double C2 protein. A review. *Biochimie* **82**: 421–426.
- Evans, T.M., and Brown, G.K. (1989). Plicate staminal filaments in *Tillandsia* subgenus *Anoplophytum*. *Am. J. Bot.* **76**: 1478–1485.
- Faria, J.M.R., Buitink, J., van Lammeren, A.A.M., and Hilhorst, H.W.M. (2005). Changes in DNA and microtubules during loss and re-establishment of desiccation tolerance in germinating *Medicago truncatula* seeds. *J. Exp. Bot.* **56**: 2119–2130.
- Furutani, I., Watanabe, Y., Prieto, R., Masukawa, M., Suzuki, K., Naoi, K., Thitamadee, S., Shikanai, T., and Hashimoto, T. (2000). The SPIRAL genes are required for directional control of cell elongation in *Arabidopsis thaliana*. *Development* **127**: 4443–4453.
- Gu, Y., Kaplinsky, N., Bringmann, M., Cobb, A., Carroll, A., Sampathkumar, A., Baskin, T.I., Persson, S., and Somerville, C. R. (2010). Identification of a cellulose synthase-associated protein required for cellulose biosynthesis. *Proc. Natl. Acad. Sci. USA* **107**: 12866–12871.
- Hamada, T., Igarashi, H., Itoh, T.J., Shimmen, T., and Sonobe, S. (2004). Characterization of a 200 kDa microtubule-associated protein of tobacco BY-2 cells, a member of the XMAP215/MOR1 family. *Plant Cell Physiol.* **45**: 1233–1242.
- Hashimoto, T. (2002). Molecular genetic analysis of left-right handedness in plants. *Philos. Trans. R. Soc. Lond. B Biol. Sci.* **357**: 799–808.
- Heath, I., and Seagull, R.W. (1982). In *The Cytoskeleton in Plant Growth and Development*, C.W. Lloyd, ed (Academic Press) 163–182.
- Ishiguro, S., Kawai-Oda, A., Ueda, J., Nishida, I., and Okada, K.

- (2001). The *DEFECTIVE IN ANther DEHISCENCE* gene encodes a novel phospholipase A1 catalyzing the initial step of jasmonic acid biosynthesis, which synchronizes pollen maturation, anther dehiscence, and flower opening in *Arabidopsis*. *Plant Cell* **13**: 2191–2209.
- Jefferson, R.A., Kavanagh, T.A., and Bevan, M.W.** (1987). GUS fusions:  $\beta$ -Glucuronidase as a sensitive and versatile gene fusion marker in higher plants. *EMBO J* **6**: 3901–3907.
- Keijzer, C.K.** (1987). The processes of anther dehiscence and pollen dispersal I. The opening mechanism of longitudinally dehiscence anthers. *New Phytol.* **105**: 487–498.
- Ketelaar, T., Anthony, R.G., and Hussey, P.J.** (2004). Green fluorescent protein-mTalin causes defects in actin organization and cell expansion in *Arabidopsis* and inhibits actin depolymerizing factor's actin depolymerizing activity in vitro. *Plant Physiol.* **136**: 3990–3998.
- Kim, S., Choi, H.I., Ryu, H.J., Park, J.H., Kim, M.D., and Kim, S.Y.** (2004). ARIA, an *Arabidopsis* arm repeat protein interacting with a transcriptional regulator of abscisic acid-responsive gene expression, is a novel abscisic acid signaling component. *Plant Physiol.* **136**: 3639–3648.
- Konishi, M., and Sugiyama, M.** (2003). Genetic analysis of adventitious root formation with a novel series of temperature-sensitive mutants of *Arabidopsis thaliana*. *Development* **130**: 5637–5647.
- Lalanne, E., Michaelidis, C., Moore, J.M., Gagliano, W., Johnson, A., Patel, R., Howden, R., Vielle-Calzada, J.P., Grossniklaus, U., and Twell, D.** (2004). Analysis of transposon insertion mutants highlights the diversity of mechanisms underlying male progamic development in *Arabidopsis*. *Genetics* **167**: 1975–1986.
- Liu, W., Xu, Z.H., Luo, D., and Xue, H.W.** (2003). Roles of OsCK1, a rice casein kinase I, in root development and plant hormone sensitivity. *Plant J.* **36**: 189–202.
- Lü, B., Gong, Z.H., Wang, J., Zhang, J.H., and Liang, J.S.** (2007). Microtubule dynamics in relation to osmotic stress-induced ABA accumulation in *Zea mays* roots. *J. Exp. Bot.* **58**: 2565–2572.
- Mandaokar, A., Thines, B., Shin, B., Lange, B.M., Choi, G., Koo, Y.J., Yoo, Y.J., Choi, Y.D., Choi, G., and Browse, J.** (2006). Transcriptional regulators of stamen development in *Arabidopsis* identified by transcriptional profiling. *Plant J.* **46**: 984–1008.
- McConn, M., and Browse, J.** (1996). The critical requirement for linolenic acid is pollen development, not photosynthesis, in an *Arabidopsis* mutant. *Plant Cell* **8**: 403–416.
- Mitsuda, N., Seki, M., Shinozaki, K., and Ohme-Takagi, M.** (2005). The NAC transcription factors NST1 and NST2 of *Arabidopsis* regulate secondary wall thickenings and are required for anther dehiscence. *Plant Cell* **17**: 2993–3006.
- Mudgil, Y., Shiu, S.H., Stone, S.L., Salt, J.N., and Goring, D.R.** (2004). A large complement of the predicted *Arabidopsis* ARM repeat proteins are members of the U-box E3 ubiquitin ligase family. *Plant Physiol.* **134**: 59–66.
- Olson, K.R., McIntosh, J.R., and Olmsted, J.B.** (1995). Analysis of MAP 4 function in living cells using green fluorescent protein (GFP) chimeras. *J. Cell Biol.* **130**: 639–650.
- Palma, K., Zhang, Y., and Li, X.** (2005). An importin alpha homolog, MOS6, plays an important role in plant innate immunity. *Curr. Biol.* **15**: 1129–1135.
- Paredes, A.R., Somerville, C.R., and Ehrhardt, D.W.** (2006). Visualization of cellulose synthase demonstrates functional association with microtubules. *Science* **312**: 1491–1495.
- Park, J.H., Halitschke, R., Kim, H.B., Baldwin, I.T., Feldmann, K.A., and Feyereisen, R.** (2002). A knock-out mutation in allene oxide synthase results in male sterility and defective wound signal transduction in *Arabidopsis* due to a block in jasmonic acid biosynthesis. *Plant J.* **31**: 1–12.
- Pignocchi, C., Minns, G.E., Nesi, N., Koumproglou, R., Kitsios, G., Benning, C., Lloyd, C.W., Doonan, J.H., and Hills, M.J.** (2009). ENDOSPERM DEFECTIVE1 is a novel microtubule-associated protein essential for seed development in *Arabidopsis*. *Plant Cell* **21**: 90–105.
- Riggleman, B., Wieschaus, E., and Schedl, P.** (1989). Molecular analysis of the armadillo locus: Uniformly distributed transcripts and a protein with novel internal repeats are associated with a *Drosophila* segment polarity gene. *Genes Dev.* **3**: 96–113.
- Robert, S., Bichet, A., Grandjean, O., Kierzkowski, D., Satiat-Jeunemaitre, B., Pelletier, S., Hauser, M.T., Höfte, H., and Vernhettes, S.** (2005). An *Arabidopsis* endo-1,4-beta-D-glucanase involved in cellulose synthesis undergoes regulated intracellular cycling. *Plant Cell* **17**: 3378–3389.
- Sakai, T., et al.** (2008). Armadillo repeat-containing kinesins and a NIMA-related kinase are required for epidermal-cell morphogenesis in *Arabidopsis*. *Plant J.* **53**: 157–171.
- Samuel, M.A., Salt, J.N., Shiu, S.H., and Goring, D.R.** (2006). Multifunctional arm repeat domains in plants. *Int. Rev. Cytol.* **253**: 1–26.
- Sanders, P.M., Bui, A.Q., Weterings, K., McIntire, K.N., Hsu, Y.C., Lee, P.Y., Truong, M.T., Beals, T.P., and Goldberg, R.B.** (1999). Anther developmental defects in *Arabidopsis thaliana* male-sterile mutants. *Sex. Plant Reprod.* **11**: 297–322.
- Sanders, P.M., Lee, P.Y., Biesgen, C., Boone, J.D., Beals, T.P., Weiler, E.W., and Goldberg, R.B.** (2000). The *Arabidopsis* *DELAYED DEHISCENCE1* gene encodes an enzyme in the jasmonic acid synthesis pathway. *Plant Cell* **12**: 1041–1061.
- Sapiro, R., Tarantino, L.M., Velazquez, F., Kiriakidou, M., Hecht, N.B., Bucan, M., and Strauss III, J.F.** (2000). Sperm antigen 6 is the murine homologue of the *Chlamydomonas reinhardtii* central apparatus protein encoded by the *PF16* locus. *Biol. Reprod.* **62**: 511–518.
- Shoji, T., Narita, N.N., Hayashi, K., Asada, J., Hamada, T., Sonobe, S., Nakajima, K., and Hashimoto, T.** (2004). Plant-specific microtubule-associated protein SPIRAL2 is required for anisotropic growth in *Arabidopsis*. *Plant Physiol.* **136**: 3933–3944.
- Smith, E.F., and Lefebvre, P.A.** (1996). *PF16* encodes a protein with armadillo repeats and localizes to a single microtubule of the central apparatus in *Chlamydomonas* flagella. *J. Cell Biol.* **132**: 359–370.
- Smith, E.F., and Lefebvre, P.A.** (2000). Defining functional domains within PF16: A central apparatus component required for flagellar motility. *Cell Motil. Cytoskeleton* **46**: 157–165.
- Smyth, D.R., Bowman, J.L., and Meyerowitz, E.M.** (1990). Early flower development in *Arabidopsis*. *Plant Cell* **2**: 755–767.
- Stintzi, A., and Browse, J.** (2000). The *Arabidopsis* male-sterile mutant, *opr3*, lacks the 12-oxophytodienoic acid reductase required for jasmonate synthesis. *Proc. Natl. Acad. Sci. USA* **97**: 10625–10630.
- Stone, S.L., Anderson, E.M., Mullen, R.T., and Goring, D.R.** (2003). ARC1 is an E3 ubiquitin ligase and promotes the ubiquitination of proteins during the rejection of self-incompatible *Brassica* pollen. *Plant Cell* **15**: 885–898.
- Tanaka, C., and Nishizuka, Y.** (1994). The protein kinase C family for neuronal signaling. *Annu. Rev. Neurosci.* **17**: 551–567.
- Twell, D., Park, S.K., Hawkins, T.J., Schubert, D., Schmidt, R., Smertenko, A., and Hussey, P.J.** (2002). MOR1/GEM1 has an essential role in the plant-specific cytokinetic phragmoplast. *Nat. Cell Biol.* **4**: 711–714.
- Ueda, K., Matsuyama, T., and Hashimoto, T.** (1999). Visualization of microtubules in living cells of transgenic *Arabidopsis thaliana*. *Protoplasma* **206**: 201–206.
- Wang, C., Li, J., and Yuan, M.** (2007). Salt tolerance requires cortical microtubule reorganization in *Arabidopsis*. *Plant Cell Physiol.* **48**: 1534–1547.
- Whittington, A.T., Vugrek, O., Wei, K.J., Hasenbein, N.G., Sugimoto, K., Rashbrooke, M.C., and Wasteneys, G.O.** (2001). MOR1 is

- essential for organizing cortical microtubules in plants. *Nature* **411**: 610–613.
- Xie, D.X., Feys, B.F., James, S., Nieto-Rostro, M., and Turner, J.G.** (1998). COI1: An *Arabidopsis* gene required for jasmonate-regulated defense and fertility. *Science* **280**: 1091–1094.
- Yang, C.Y., Xu, Z.Y., Song, J., Conner, K., Vizcay Barrena, G., and Wilson, Z.A.** (2007). *Arabidopsis* MYB26/MALE STERILE35 regulates secondary thickening in the endothecium and is essential for anther dehiscence. *Plant Cell* **19**: 534–548.
- Yasuor, H., Abu-Abied, M., Belausov, E., Madmony, A., Sadot, E., Riov, J., and Rubin, B.** (2006). Glyphosate-induced anther indehiscence in cotton is partially temperature dependent and involves cytoskeleton and secondary wall modifications and auxin accumulation. *Plant Physiol.* **141**: 1306–1315.
- Zhao, D.Z., and Ma, H.** (2000). Male fertility: A case of enzyme identity. *Curr. Biol.* **10**: R904–R907.
- Zhu, Q.H., Ramm, K., Shivakkumar, R., Dennis, E.S., and Upadhyaya, N.M.** (2004). The ANTH<sup>ER</sup> INDEHISCENCE1 gene encoding a single MYB domain protein is involved in anther development in rice. *Plant Physiol.* **135**: 1514–1525.